Eur. Phys. J. A **23**, 305–315 (2005)
DOI 10.1140/epja/i2004-10082-0

THE EUROPEAN PHYSICAL JOURNAL A

Dynamical chiral-symmetry breaking at T = 0 and T ≠ 0 in the Schwinger-Dyson equation with lattice QCD data

H. Iida[a], M. Oka, and H. Suganuma

Faculty of Science, Tokyo Institute of Technology, Ohkayama 2-12-1, Meguro, Tokyo 152-8551, Japan

Received: 17 May 2004 / Revised version: 4 August 2004 /
Published online: 3 December 2004 –
Communicated by U.-G. Meißner

Abstract. Dynamical chiral-symmetry breaking (DCSB) in QCD is investigated in the Schwinger-Dyson (SD) formalism based on lattice QCD data. From the quenched lattice data for the quark propagator in the Landau gauge, we extract the SD integral kernel function, the product of the quark-gluon vertex and the polarization factor in the gluon propagator, in an Ansatz-independent manner. We find that the SD kernel function exhibits the characteristic behavior of nonperturbative physics, such as infrared vanishing and strong enhancement at the intermediate-energy region around $p \sim 0.6\,\mathrm{GeV}$. The infrared and intermediate energy region ($0.4\,\mathrm{GeV} < p < 1.5\,\mathrm{GeV}$) is found to be most relevant for DCSB from analysis on the relation between the SD kernel and the quark mass function. We apply the lattice-QCD–based SD equation to thermal QCD, and calculate the quark mass function at the finite temperature. Spontaneously broken chiral symmetry is found to be restored at high temperature above 110 MeV.

PACS. 12.38.Aw General properties of QCD (dynamics, confinement, etc.) – 12.38.Lg Other nonperturbative calculations – 12.38.Mh Quark-gluon plasma – 12.38.-t Quantum chromodynamics

1 Introduction

Quantum chromodynamics (QCD) has been accepted as the fundamental theory of the strong interaction of hadrons. Due to the asymptotic freedom of QCD, the perturbative calculation is applicable to the high-energy process in the hadron reactions. In contrast, low-energy QCD becomes a strong-coupling gauge theory, and exhibits interesting nonperturbative phenomena such as color confinement and dynamical chiral-symmetry breaking (DCSB) [1–3].

The QCD running coupling constant $\alpha_s(p^2)$ is governed by the QCD scale parameter, $\Lambda_{\mathrm{QCD}}(\overline{\mathrm{MS}}) = 216 \pm 25\,\mathrm{MeV}$, evaluated in the $\overline{\mathrm{MS}}$ scheme of the perturbative QCD with $N_f = 5$ [4]. A rough perturbative estimation leads to $\alpha_s((0.5\,\mathrm{GeV})^2) \sim 1$, which suggests that the perturbation theory would break down at around $p \sim 0.5\,\mathrm{GeV}$. In other words, this is expected to be the momentum scale in which nonperturbative effects appear due to the strong coupling.

DCSB is one of the outstanding nonperturbative features in QCD. The chiral symmetry, which the QCD Lagrangian possesses in the massless quark limit, is spontaneously broken in the nonperturbative QCD vacuum. The nontrivial QCD vacuum is characterized by the quark condensate $\langle\bar{q}q\rangle \simeq -(225 \pm 25\,\mathrm{MeV})^3$ [5], which is caused by attractive interaction acting on the quark-antiquark pair like Cooper-pair condensation in superconductivity [1]. Dynamical content of DCSB has been demonstrated by using the effective models of QCD such as the Nambu-Jona-Lasinio model [1,6] and the instanton vacuum model [7]. These models suggest that the almost massless quark acquires a large effective mass of $M \simeq 300\,\mathrm{MeV}$ as a result of DCSB and behaves as a massive constituent quark [8] in the infrared region. The pion is identified as the Nambu-Goldstone boson associated with DCSB and satisfies the low-energy theorem [9], where the pion decay constant, $f_\pi \simeq 93\,\mathrm{MeV}$, is also a relevant quantity characterizing DCSB. In this way, DCSB is characterized by several quantities, the quark condensate $\langle\bar{q}q\rangle \simeq -(225 \pm 25\,\mathrm{MeV})^3$, the effective quark mass $M \simeq 300\,\mathrm{MeV}$ and the pion decay constant $f_\pi \simeq 93\,\mathrm{MeV}$.

In the study of DCSB based on QCD, the Schwinger-Dyson (SD) equation [2,3,10–12] and the Bethe-Salpeter equation [13], which are expressed as integral equations, have been used to incorporate infinite-order effects on the gauge coupling. One of the most popular approaches, however, is to use the free gluon propagator and the one-loop running coupling for the quark-gluon vertex in the SD equation. This simplification may result in neglecting possible nonperturbative effects in the infrared region. In several studies, the infrared nonperturbative effect was

[a] e-mail: iida@th.phys.titech.ac.jp

modeled and was taken into account in the SD equation [14–16], but the models contains some unjustified assumptions. Another standard method to incorporate nonperturbative effects is lattice QCD. Numerical evaluation of the chiral condensate on the lattice shows DCSB. It also shows chiral symmetry restoration at finite temperature [17]. Recently, the nonperturbative quark and gluon propagators have been calculated in lattice QCD Monte Carlo simulations. They motivated the present study.

In this paper, we attempt to combine the SD approach and the lattice QCD result for the quark and gluon propagators as the first step of understanding the hadron physics in terms of quarks and gluons. Our aim is to include information from lattice QCD calculation as much as possible to the SD equation and to investigate the properties of DCSB and its constraints on the various characteristic scales mentioned above. In the course of this study, we find that a strong enhancement is necessary in the integral kernel of the SD equation, which indicates the indispensable role of nonperturbative physics at medium and low momentum area. We further investigate the behaviors of the solution of the SD equation at finite temperature including the most fundamental temperature dependences of the integral kernel and the quark propagator.

The paper is organized as follows. In sect. 2, the quark and the gluon propagators resulted from lattice QCD calculations and their parameterizations for our calculation are presented. In sect. 3, formulation of the SD equation of the quark propagator for Euclidean momenta is presented. We fix the gauge to the Landau gauge according to the lattice calculation and assume dominance of the Lorentz vector part of the gluon-quark vertex. Then we define the integral kernel function for the Landau-gauge SD equation, which corresponds to the product of the quark-gluon vertex and the polarization factor in the full gluon propagator. In sect. 4, we use the lattice QCD data of the quark propagator and invert the SD equation to extract the kernel function and study its properties. In sect. 5, we consider various modifications of the SD kernels in order to identify which part of the propagator is most responsible for DCSB. In sect. 6, the SD equation is solved for finite temperature and the results are presented. Section 7 is devoted to the summary and concluding remarks.

2 Propagators of quarks and gluons in lattice QCD

In this section, we summarize the recent lattice QCD results for the quark and the gluon propagators. The lattice QCD Monte Carlo simulation is the first principle calculation of the strong interaction directly based on QCD in the Euclidean metric. In these years, lattice QCD calculations have been performed for the quark and gluon propagators in the Landau gauge at the quenched level [18–20]. These propagators are considered to include all the nonperturbative effects in quenched QCD.

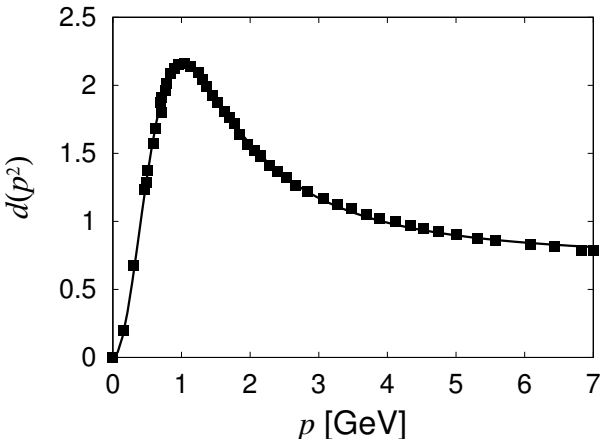

Fig. 1. The lattice QCD result for the polarization factor $d(q^2) = q^2 D(q^2)$ in the gluon propagator in the Landau gauge. The symbols denote the lattice data taken from ref. [18], and the curve denotes the fit function of $d(p^2)$ in eq. (2).

The Euclidean gluon propagator in the Landau gauge is generally expressed by

$$D_{\mu\nu}(p^2) = \frac{d(p^2)}{p^2}\left(\delta_{\mu\nu} - \frac{p_\mu p_\nu}{p^2}\right), \tag{1}$$

where we refer to $d(p^2)$ as the "polarization factor" in the nonperturbative gluon propagator.

We find that the quenched lattice QCD data [18] for the polarization factor $d(p^2)$ is well described by the analytic function of

$$d(p^2) = Z_g \frac{p^4 + ap^2}{p^4 + \alpha p^2 + \beta} \tag{2}$$

with $a \simeq 7.887\,\mathrm{GeV}^2$, $\alpha \simeq 1.254\,\mathrm{GeV}^2$, $\beta \simeq 0.7175\,\mathrm{GeV}^4$ and $Z_g \simeq 0.7172$, as shown in fig. 1. (In the first reference of [18], the lattice data are set to satisfy $d(p^2) = 1$ at the typical lattice cutoff $p = 4\,\mathrm{GeV}$.)

Note here that there are two remarkable features in the functional shape of $d(p^2)$.

1. The polarization factor $d(p^2)$ exhibits the infrared vanishing and $d(p^2)$ is proportional to p^2 in the infrared region as $p < 0.5\,\mathrm{GeV}$.
2. The polarization factor $d(p^2)$ exhibits a large enhancement in the intermediate-energy region as $p \sim 1\,\mathrm{GeV}$.

Next, we summarize the quark propagator $S(p)$ in the Landau gauge in lattice QCD. The Euclidean quark propagator in the Landau gauge is generally expressed as

$$S(p) = \frac{Z(p^2)}{\not{p} + M(p^2)}, \tag{3}$$

with the quark mass function $M(p^2)$ and the quark wave function renormalization factor $Z(p^2)$ [2,3]. In terms of the quark propagator, DCSB is characterized by the mass generation as $M(p^2) \neq 0$.

The quark mass function $M(p^2)$ in the Landau gauge is recently measured in lattice QCD at the quenched level [19,20], and is reported to be fitted as

$$M(p^2) = \frac{M_0}{1 + (p/\bar{p})^\gamma} \tag{4}$$

with $M_0 \simeq 260$ MeV, $\bar{p} \simeq 870$ MeV and $\gamma \simeq 3.04$ [19] in the range of $0 \leq p \leq 4\,\mathrm{GeV}$ in the chiral limit. The infrared quark mass $M(0) = M_0 \simeq 260\,\mathrm{MeV}$ seems consistent with the constituent quark mass in the quark model [8]. Note that the lattice results of the quark mass function may have ambiguity coming from the chiral extrapolation. In ref. [19], eq. (4) was obtained by the linear chiral extrapolation of the lattice data. In ref. [21], however, the authors claimed that the results may change if they employ an analytic extrapolation towards the chiral limit, although it depends on the choice of mass dependence of the fitting functions.

As for the quark wave-function renormalization factor $Z(p^2)$ in the Landau gauge, the lattice QCD data [19, 20] show $Z(p^2) < 1$ for small p below a few GeV, and $Z(p^2) \simeq 1$ for large p. Quantitatively, the lattice QCD data [19,20] seem to be fitted as

$$Z(p^2) = 1 - \frac{cp_0^2}{p^2 + p_0^2} \tag{5}$$

with $p_0 \simeq 1.0\,\mathrm{GeV}$ and $c \simeq 0.3$, although the lattice data themselves seem somehow unsettled due to the relatively large statistical error and the systematic error such as a large lattice-fermion dependence [19,20]. In this paper, we adopt eq. (5) for the main calculations, and investigate the effects of the quark wave-function renormalization by comparing with the calculation with $Z(p^2) = 1$.

3 The Schwinger-Dyson formalism for quarks

The Schwinger-Dyson (SD) equation for the quark propagator $S(p)$ is described with the nonperturbative gluon propagator $D_{\mu\nu}(p)$ and the nonperturbative quark-gluon vertex $g\Gamma_\nu(p,q)$ as

$$S^{-1}(p) = S_0^{-1}(p) + C_F g^2 \int \frac{\mathrm{d}^4 q}{(2\pi)^4} \gamma_\mu S(q) D_{\mu\nu}(p-q) \Gamma_\nu(p,q) \tag{6}$$

in the Euclidean metric. Here, $S_0(p)$ denotes the bare quark propagator, and the color factor of quarks has been calculated as $C_F = 4/3$.

In several studies for QCD, however, the SD formalism is drastically truncated: the perturbative gluon propagator and the one-loop running coupling are used instead of the nonperturbative quantities in the original formalism. This simplification seems rather dangerous because some of the nonperturbative-QCD effects are neglected.

We formulate the SD equation for quarks in the chiral limit in the Landau gauge. By taking the trace of eq. (6), one finds

$$\frac{M(p^2)}{Z(p^2)} = \frac{C_F g^2}{4} \int \frac{\mathrm{d}^4 q}{(2\pi)^4} D_{\mu\nu}(p-q) \times \mathrm{tr}\left\{ \gamma_\mu \frac{Z(q^2)}{\not{q} + M(q^2)} \Gamma_\nu(p,q) \right\}. \tag{7}$$

For the quark-gluon vertex $\Gamma(p,q)$, one of the desirable direction is to use the lattice QCD data. Recently, a pioneering lattice result was reported for the quark-gluon vertex $\Gamma(p,q)$ [22]. At present, however, only limited information for the vertex $\Gamma(p,q)$ is obtained from the lattice QCD such as $\Gamma(p,p)$. For the actual calculation of the SD equation (7), the full information of $\Gamma(p,q)$ is necessary, and therefore the present lattice result for the quark-gluon vertex is not applicable. In addition, no conclusive vertex form is known yet, although several vertex Ansätze are theoretically proposed [23–25].

Therefore, we assume the chiral-preserving vector-type vertex,

$$\Gamma_\mu(p,q) = \gamma_\mu \Gamma((p-q)^2), \tag{8}$$

which keeps the chiral symmetry properly. Here, this type of quark-gluon vertex and its approximate form with the Higashijima-Miransky approximation [2,3] have been frequently used in the studies with the SD equation. Note also that, to preserve the Ward-Takahashi identity for the axial vector vertex, the gluon momentum $(p-q)$ should be taken as the argument of the quark-gluon vertex Γ in the ladder approximation of the SD and BS equations [26]. In contrast, to be strict, the Higashijima-Miransky approximation explicitly breaks the chiral symmetry in the formalism [26].

Using the vector-type quark-gluon vertex in eq. (8), one obtains

$$\frac{M(p^2)}{Z(p^2)} = C_F g^2 \int \frac{\mathrm{d}^4 q}{(2\pi)^4} \frac{Z(q^2) M(q^2)}{q^2 + M^2(q^2)} \times \Gamma((p-q)^2) D_{\mu\mu}((p-q)^2). \tag{9}$$

In the Landau gauge, the Euclidean gluon propagator takes the general form of eq. (1) with the gluon polarization factor $d(p^2)$. Therefore, eq. (9) is expressed as

$$\frac{M(p^2)}{Z(p^2)} = 3C_F g^2 \int \frac{\mathrm{d}^4 q}{(2\pi)^4} \frac{Z(q^2) M(q^2)}{q^2 + M^2(q^2)} \times \frac{\Gamma((p-q)^2) d((p-q)^2)}{(p-q)^2}. \tag{10}$$

Here, we define the kernel function

$$K(p^2) \equiv g^2 \Gamma(p^2) d(p^2) \tag{11}$$

as the product of the quark-gluon vertex $\Gamma(p^2)$ and the gluon polarization factor $d(p^2)$. Then, the SD equation is rewritten as

$$\frac{M(p^2)}{Z(p^2)} = 3C_F \int \frac{\mathrm{d}^4 q}{(2\pi)^4} \frac{Z(q^2) M(q^2)}{q^2 + M^2(q^2)} \frac{K((p-q)^2)}{(p-q)^2}. \tag{12}$$

Note that the precise SD kernel $\hat{K}_{\rm SD}(p^2)$ of the SD equation includes the Coulomb-propagator factor $1/p^2$ as

$$\hat{K}_{\rm SD}(p^2) \equiv \frac{K(p^2)}{p^2} = \frac{g^2\Gamma(p^2)d(p^2)}{p^2}. \quad (13)$$

In the Landau gauge, several studies use the approximation of $Z(p^2) = 1$ [2,13,26]. In this approximation, the SD equation reduces to

$$M(p^2) = 3C_F \int \frac{{\rm d}^4q}{(2\pi)^4} \frac{M(q^2)}{q^2 + M^2(q^2)} \frac{K((p-q)^2)}{(p-q)^2}. \quad (14)$$

4 Extraction of the kernel function in the SD equation from lattice QCD

In most case, the SD equation is used to calculate the quark propagator using the gluon propagator and the quark-gluon vertex [2,3]. However, the SD equation is nothing but the relation among the gluon propagator, the quark-gluon vertex and the quark propagator.

Then, we find that the SD kernel, the product of the gluon propagator and the quark-gluon vertex, can be extracted from the information of the quark propagator using the SD equation (12). In fact, once the quark propagator is obtained, the SD kernel function $K(p^2)$ can be extracted without any assumption on the functional form of $\Gamma(p^2)$ or $K(p^2)$.

In this section, we extract the kernel function $K(p^2) = g^2\Gamma(p^2)d(p^2)$ in the SD equation (12) from the quark propagator obtained in lattice QCD, *i.e.*, the quark mass function $M(p^2)$ in eq. (4) and the quark wave-function renormalization factor $Z(p^2)$ in eq. (5), in an Ansatz-independent manner.

4.1 Formalism

By shifting the integral variable from q to $\tilde{q} \equiv p - q$, we rewrite eq. (12) as

$$\frac{M(p^2)}{Z(p^2)} = 3C_F \int \frac{{\rm d}^4\tilde{q}}{(2\pi)^4} \frac{Z((p-\tilde{q})^2)M((p-\tilde{q})^2)}{(p-\tilde{q})^2 + M^2((p-\tilde{q})^2)} \frac{K(\tilde{q}^2)}{\tilde{q}^2}. \quad (15)$$

Therefore, we obtain

$$\frac{M(p^2)}{Z(p^2)} = \int_0^\infty {\rm d}\tilde{q}^2 \Theta(p^2, \tilde{q}^2) K(\tilde{q}^2), \quad (16)$$

where $\Theta(p^2, q^2)$ is defined with $M(p^2)$ as

$$\Theta(p^2, q^2) \equiv \frac{3C_F}{8\pi^3} \int_0^\pi {\rm d}\theta \sin^2\theta \times \frac{Z(p^2+q^2-2pq\cos\theta)M(p^2+q^2-2pq\cos\theta)}{p^2+q^2-2pq\cos\theta + M^2(p^2+q^2-2pq\cos\theta)}. \quad (17)$$

Regarding the momentum squared (p^2, $\tilde{q}^2$) as suffixes (m, n), eq. (16) can be rewritten as

$$\frac{M_m}{Z_m} = \sum_n \Theta_{mn} K_n. \quad (18)$$

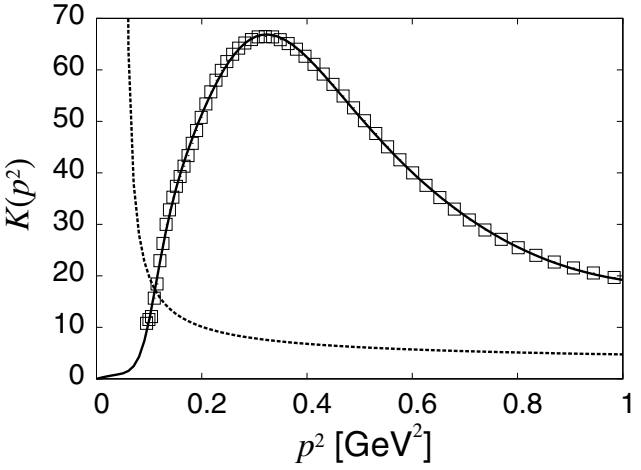

Fig. 2. The kernel function in the SD equation, $K(p^2) = g^2\Gamma(p^2)d(p^2)$, extracted from the lattice QCD result of the quark propagator in the Landau gauge. The calculated data are denoted by the square symbols, and the solid curve denotes the fit function in eq. (22). The dotted curve denotes the perturbative SD kernel function $K_{\rm pert}(p^2)$ for comparison. As remarkable features, $K(p^2)$ exhibits infrared vanishing and intermediate enhancement.

Here, Θ_{mn} is a real symmetric matrix on m and n as

$$\Theta_{mn} = \Theta_{nm} \in \mathbf{R}, \quad (19)$$

because of $\Theta(p^2, q^2) = \Theta(q^2, p^2) \in \mathbf{R}$.

Once the quark mass function $M(p^2)$ and the quark wave function renormalization factor $Z(p^2)$ are obtained, $\Theta(p^2, q^2)$ is calculable with eq. (17), and, using eq. (18), we can extract K_n directly from Θ_{mn} and M_n as

$$K_m = \sum_n \Theta^{-1}_{mn} \frac{M_n}{Z_n}. \quad (20)$$

Since $M(p^2)$ and $Z(p^2)$ are given by eqs. (4) and (5) in lattice QCD, we can calculate the kernel function $K(p^2)$ from eq. (20) without any assumption of the functional form on $K(p^2)$. For the practical calculation, we discretize the momentum squared p^2 and $\tilde{q}^2$ after the proper transformation as $p^2 = \tan^4\alpha$ and $\tilde{q}^2 = \tan^4\beta$, and solve eq. (18) for K_n. (See appendix for details.)

The shift of the integration variable in eq. (15) can be done in the case that the integral is finite. On this point, the integral of the right-hand side of eq. (15) must be finite since the left-hand side is obviously finite. Therefore, we can shift the integration variable safely in eq. (15).

4.2 Numerical result for the kernel function

As shown in fig. 2, we numerically extract the kernel function $K(p^2) = g^2\Gamma(p^2)d(p^2)$ from the lattice QCD result, eqs. (4) and (5), for the quark propagator in the Landau gauge. For the check of the validity, we have confirmed that the mass function $M(p^2)$ in eq. (4) is precisely reproduced with the obtained kernel function $K(p^2)$.

As remarkable features, we find "infrared vanishing" and "intermediate enhancement" in the kernel function $K(p^2)$ in the SD equation [27]:

1. The SD kernel function $K(p^2)$ seems consistent with zero in the very infrared region as

$$K(p^2 < 0.1\,\mathrm{GeV}^2) \simeq 0. \tag{21}$$

2. The SD kernel function $K(p^2)$ exhibits a large enhancement in the intermediate-energy region around $p \sim 0.6$ GeV. In fact, $K(p^2)$ takes the maximal value $K_{\max} = 66.86$ at $p^2 \simeq 0.321\,\mathrm{GeV}^2 \simeq (0.607\,\mathrm{GeV})^2$.

These tendencies of infrared vanishing and intermediate enhancement in the kernel function $K(p^2) = g^2\Gamma(p^2)d(p^2)$ are qualitatively observed also in the direct lattice-QCD measurement for the polarization factor $d(p^2)$ in the gluon propagator in the Landau gauge [18] as shown in fig. 1, although the peak position between $K(p^2)$ and $d(p^2)$ is largely different. (The shape of the obtained kernel function $K(p^2)$ is also similar to that in refs. [21] and [28] using a model gluon propagator in terms of infrared vanishing and intermediate enhancement, although there is some quantitative difference on the peak position.)

Note here that we have *never* used the information of the gluon propagator such as $d(p^2)$ in extracting the kernel function $K(p^2)$. Actually, we *only* use the quark propagator to extract the SD kernel $K(p^2)$. Nevertheless, we find in $K(p^2)$ the similar tendencies to $d(p^2)$, which is rather nontrivial.

In other words, the properties of infrared vanishing and intermediate enhancement in the SD kernel function $K(p^2)$ are embedded in the information of the quark propagator, *i.e.*, $M(p^2)$ and $Z(p^2)$ in eqs. (4) and (5), in an implicit manner.

The original lattice data for the quark propagator are limited in the momentum region below 4 GeV due to the finite lattice spacing. We note however that our obtained SD kernel $K(p^2)$ exhibits a clear perturbative logarithmic behavior in the momentum region of $2.5\,\mathrm{GeV} < p < 4\,\mathrm{GeV}$, and it is rather difficult to reproduce the SD kernel $K(p^2)$ without the perturbative logarithmic denominator.

As a simple parametrization, the obtained SD kernel function $K(p^2)$ in the region of $0 \leq p \leq 4\,\mathrm{GeV}$ can be fitted fairly well by

$$K(p^2) = \frac{G(p^2)}{F(p^2)} \cdot \frac{1}{\beta_0 \ln\{(p^2 + p_c^2)/\Lambda_{\mathrm{QCD}}^2\}}, \tag{22}$$

with $\Lambda_{\mathrm{QCD}} = 220\,\mathrm{MeV}$, $\beta_0 \equiv \frac{(11N_c - 2N_f)}{48\pi^2} = \frac{11}{16\pi^2}$ and an infrared cutoff $p_c \simeq 2.207\Lambda_{\mathrm{QCD}}$. Here, $F(p^2)$ and $G(p^2)$ are some polynomials of p^2: $F(p^2) = \sum_{n=0}^{6} f_n (p^2)^n$ and $G(p^2) = \sum_{n=1}^{6} g_n (p^2)^n$ with $f_0 = 0.001495$, $f_1 = -0.03227$, $f_2 = 0.2812$, $f_3 = -1.121$, $f_4 = 2.462$, $f_5 = -2.498$, $f_6 = 1$, $g_1 = 0.008746$, $g_2 = -0.2288$, $g_3 = 2.020$, $g_4 = -1.192$, $g_5 = -2.265$, $g_6 = 2.134$ in the unit of GeV^{-2n}. We show this fit function by the solid curve in fig. 2.

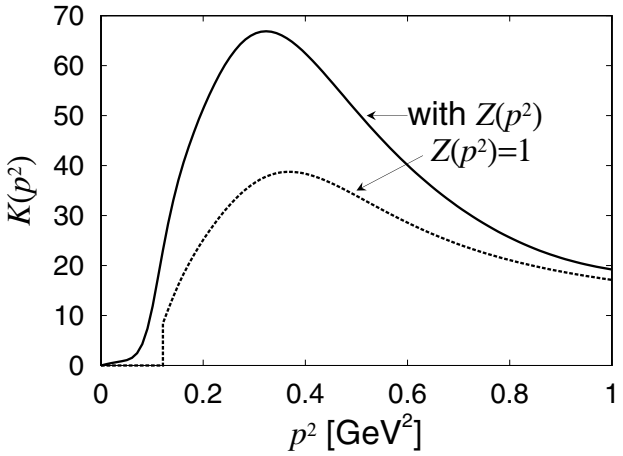

Fig. 3. The kernel function in the SD equation, $K(p^2) = g^2\Gamma(p^2)d(p^2)$, extracted from the lattice QCD result of the quark mass function $M(p^2)$ with $Z(p^2) = 1$ in the Landau gauge (dotted line) and the solid line is the kernel function with $Z(p^2) \neq 1$ for comparison. Even with $Z(p^2) = 1$, $K(p^2)$ exhibits infrared vanishing and intermediate enhancement.

4.3 The effect of the quark wave-function renormalization to the SD kernel

To investigate the effect of the quark wave function renormalization, we calculate the kernel function $K(p^2)$ from $M(p^2)$ with fixed $Z(p^2) = 1$, and show the result in fig. 3. $K(p^2)$ with $Z(p^2) = 1$ takes the maximal value $K_{\max} = 38.76$ at $p^2 \simeq 0.368\,\mathrm{GeV}^2 \simeq (0.607\,\mathrm{GeV})^2$.

Even with fixed $Z(p^2) = 1$, the kernel function $K(p^2)$ exhibits infrared vanishing and intermediate enhancement, which indicates that these two properties of $K(p^2)$ originate from the behavior of the quark mass function $M(p^2)$ rather than the quark wave function renormalization.

Actually, the kernel function $K(p^2)$ obtained with $Z(p^2) = 1$ is rather similar to that obtained with $Z(p^2)$ in eq. (5) in the infrared region, and the effect of the quark wave-function renormalization factor $Z(p^2)$ appears as an overall factor multiplication to the kernel function $K(p^2)$ in the infrared region.

In this way, the shape of the quark mass function $M(p^2)$ in eq. (4) is considered to correlate with infrared vanishing and intermediate enhancement in the SD kernel.

4.4 Comparison with the one-loop ladder approximation

As a popular approach in the SD equation, the perturbative gluon propagator with $d(p^2) = 1$ and the one-loop running coupling $g_{\mathrm{run}}(p^2)$ are frequently used [2,3], and this treatment corresponds to the usage of the perturbative SD kernel function,

$$K_{\mathrm{pert}}(p^2) = g_{\mathrm{run}}^2(p^2) = \frac{1}{\beta_0 \ln(p^2/\Lambda_{\mathrm{QCD}}^2)}. \tag{23}$$

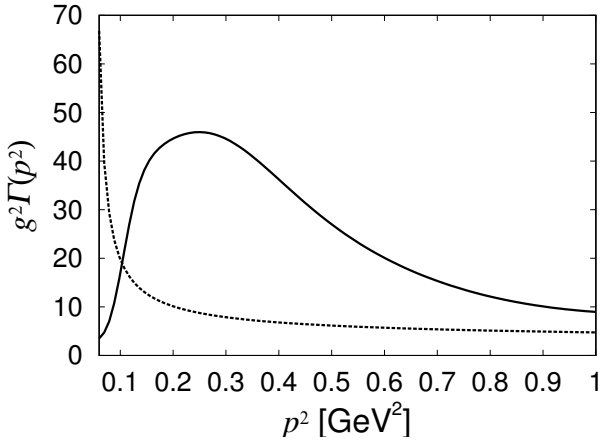

Fig. 4. The quark-gluon vertex function $g^2\Gamma(p^2)$. For comparison, the perturbative quark-gluon vertex $g^2_{\rm run}(p^2)$ in the ladder approximation is also plotted by the dotted curve. $g^2\Gamma(p^2)$ shows intermediate enhancement.

For comparison, we add by the dotted curve in fig. 3 the perturbative SD kernel function $K_{\rm pert}(p^2)$ at the one-loop level with $\Lambda_{\rm QCD} = 220\,{\rm MeV}$ and $N_f = 0$ at the quenched level. Both in the infrared and in the intermediate energy regions, $K_{\rm pert}(p^2)$ largely differs from the present result $K(p^2)$ based on lattice QCD. In fact, the simple version of the SD equation using the perturbative gluon propagator and the one-loop running coupling would be too crude for the quantitative study of QCD.

4.5 The quark-gluon vertex function

Here, we extract the quark gluon-vertex function from the obtained SD kernel function and the gluon propagator calculated by lattice QCD. Using eq. (11), the quark-gluon vertex $g^2\Gamma(p^2)$ is obtained from our obtained SD kernel $K(p^2)$ and the gluon polarization factor $d(p^2)$ in eq. (2) as

$$g^2\Gamma(p^2) = K(p^2)/d(p^2). \qquad (24)$$

We show in fig. 4 the quark-gluon vertex function $g^2\Gamma(p^2)$. For comparison, we also plot in fig. 4 the perturbative quark-gluon vertex function $g^2_{\rm run}(p^2)$ in the ladder approximation.

The quark-gluon vertex $g^2\Gamma(p^2)$ exhibits intermediate enhancement around $p^2 \sim 0.25\,{\rm GeV}^2$, *i.e.*, $p \sim 0.5\,{\rm GeV}$, in comparison with $g^2_{\rm run}(p^2)$, and seems to decrease in the infrared region as $p^2 < 0.2\,{\rm GeV}^2$. Note however that the obtained quark-gluon vertex $g^2\Gamma(p^2)$ would be reliable only for the region of $p^2 \geq 0.1\,{\rm GeV}^2$, because both $d(p^2)$ and $K(p^2)$ are rather small in the ultra-infrared region of $p^2 < 0.1\,{\rm GeV}^2$ and the ratio in eq. (24) becomes uncertain there in due to the numerical errors in lattice QCD.

5 Relation between DCSB and the SD kernel

In this section, we investigate the correspondence between the quark mass function $M(p^2)$ and the SD kernel function $K(p^2)$, and discuss the relevant momentum region for DCSB. In actual, we calculate the quark mass functions for the following modified SD kernels:

1. An ultraviolet (UV) cutoff for the SD kernel
2. An infrared (IR) cutoff for the SD kernel
3. An intermediate (IM) suppression for the SD kernel

Through the investigation of the UV-cut case, the IR-cut case and the IM-suppression case for the SD kernel, we numerically estimate the relevant momentum region for DCSB. (Note that it is difficult to find out such relevant region in a direct and rigorous manner due to the nonlinearity of the SD equation.) For simplicity, we perform these calculations using the SD equation (14) with $Z(p^2) = 1$, considering inaccuracy of the present lattice data for the wave function renormalization $Z(p^2)$.

To begin with, we investigate the role of UV region for DCSB by examining the UV-cut case for the SD

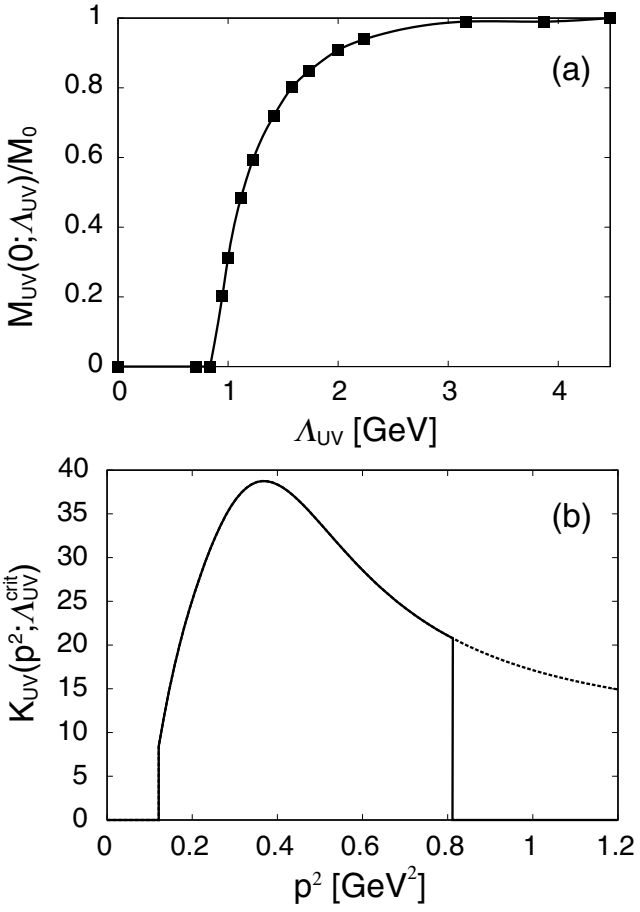

Fig. 5. (a) The infrared quark mass $M_{\rm UV}(0;\Lambda_{\rm UV})/M_0$ in the UV-cut SD equation plotted against the artificial UV-cutoff parameter $\Lambda_{\rm UV}$. $M_0 \simeq 260\,{\rm MeV}$ denotes the infrared quark mass. For $\Lambda_{\rm UV} > 2\,{\rm GeV}$, almost no effect is observed. For $\Lambda_{\rm UV} < \Lambda^{\rm crit}_{\rm UV} \simeq 0.9\,{\rm GeV}$, no DCSB is observed as $M_{\rm UV}(p^2;\Lambda_{\rm UV}) = 0$. (b) The UV-cut SD kernel $K_{\rm UV}(p^2;\Lambda^{\rm crit}_{\rm UV})$ for the critical case on DCSB. The dotted curve denotes the original SD kernel function $K(p^2)$.

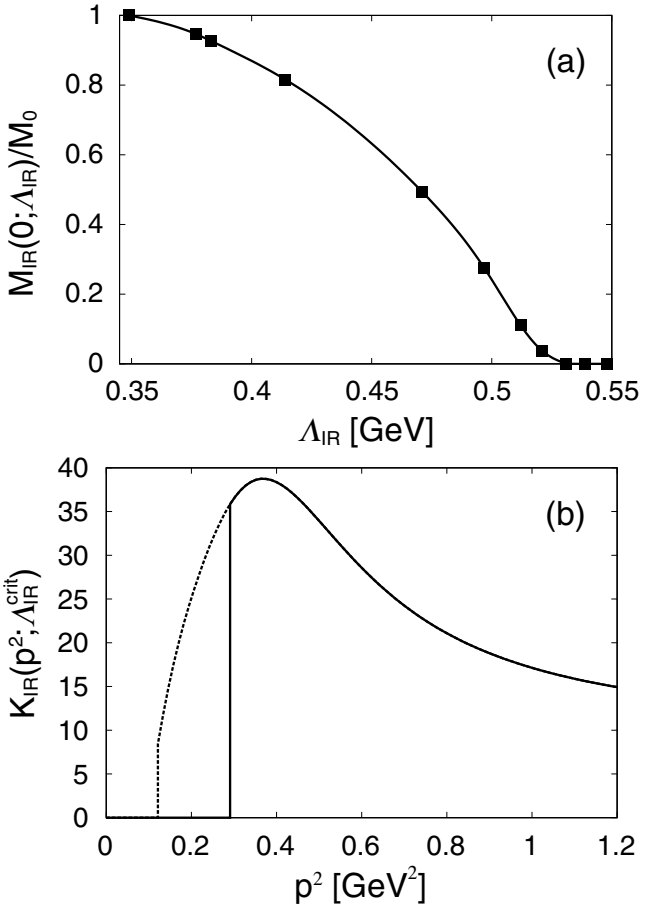

Fig. 6. (a) The infrared quark mass $M_{\rm IR}(0;\Lambda_{\rm IR})/M_0$ in the IR-cut SD equation plotted against the artificial IR-cutoff parameter $\Lambda_{\rm IR}$. For $\Lambda_{\rm IR}$ <0.4GeV, there is no significant effect observed for DCSB. For $\Lambda_{\rm IR} > \Lambda_{\rm IR}^{\rm crit} \simeq 0.53\,{\rm GeV}$, no DCSB is observed as $M_{\rm IR}(p^2;\Lambda_{\rm IR}) = 0$. (b) The IR-cut SD kernel $K_{\rm IR}(p^2;\Lambda_{\rm IR}^{\rm crit})$ for the critical case on DCSB. The dotted curve denotes the original SD kernel function $K(p^2)$.

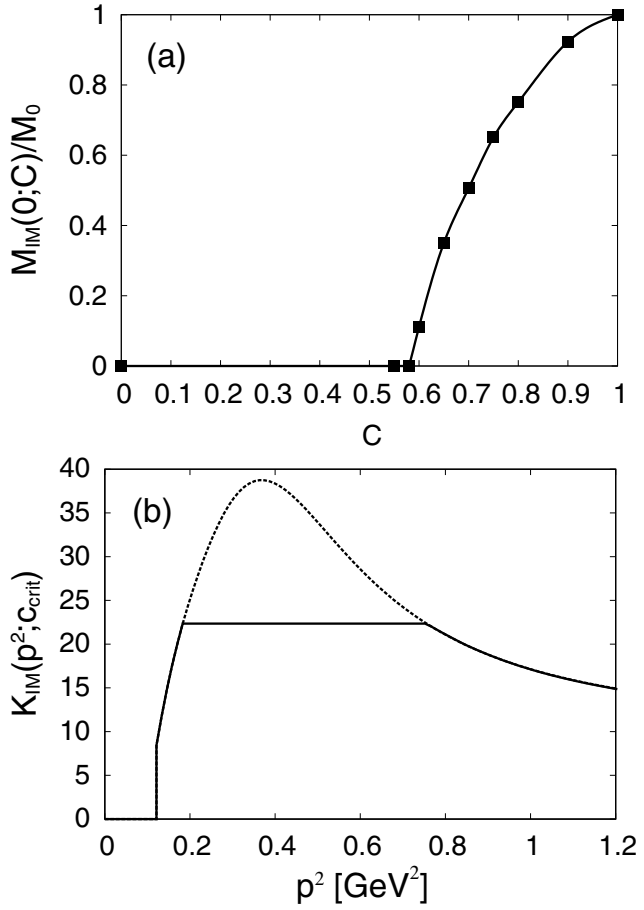

Fig. 7. (a) The infrared quark mass $M_{\rm IM}(0;c)/M_0$ in the IM-suppressed SD equation plotted against the artificial IM-suppression parameter c. No DCSB is found as $M_{\rm IM}(p^2;c) = 0$ for $c < c_{\rm crit} \simeq 0.58$. (b) The IM-suppressed SD kernel $K_{\rm IM}(p^2;c_{\rm crit})$ for the critical case on DCSB. The dotted curve denotes the original SD kernel function $K(p^2)$.

equation (14). Here, we use the UV-cut SD kernel function,

$$K_{\rm UV}(p^2;\Lambda_{\rm UV}) \equiv K(p^2)\theta(\Lambda_{\rm UV}^2 - p^2), \qquad (25)$$

instead of $K(p^2)$. For each $\Lambda_{\rm UV}$, we solve the UV-cut SD equation and obtain the corresponding solution $M_{\rm UV}(p^2;\Lambda_{\rm UV})$ for the quark mass function. We show in fig. 5(a) the infrared quark mass $M_{\rm UV}(0;\Lambda_{\rm UV})$ plotted against $\Lambda_{\rm UV}$. For $\Lambda_{\rm UV} > 2\,{\rm GeV}$, almost no effect is observed as $M_{\rm UV}(p^2;\Lambda_{\rm UV}) \simeq M_{\rm UV}(p^2;\infty) = M(p^2)$, which clearly indicates that UV region is not important for DCSB. In contrast, a significant reduction of the quark mass function $M_{\rm UV}(p^2;\Lambda_{\rm UV})$ is observed for $\Lambda_{\rm UV} < 1.5\,{\rm GeV}$. In particular, for $\Lambda_{\rm UV} < \Lambda_{\rm UV}^{\rm crit} \simeq 0.9\,{\rm GeV}$, no DCSB is observed as $M_{\rm UV}(p^2;\Lambda_{\rm UV}) = 0$, which may suggest that the momentum scale of $p \sim 1\,{\rm GeV}$ plays an important role for DCSB. Figure 5(b) shows the UV-cut SD kernel function for $\Lambda_{\rm UV}^{\rm crit}$, which is the critical value on DCSB. This result seems natural because the strong-coupling nature at the infrared and intermediate energy regions would be essential for DCSB in QCD [15,21].

Next, we investigate the role of IR region for DCSB by examining the IR-cut case with the IR-cut SD kernel function,

$$K_{\rm IR}(p^2;\Lambda_{\rm IR}) \equiv K(p^2)\theta(p^2 - \Lambda_{\rm IR}^2). \qquad (26)$$

For each $\Lambda_{\rm IR}$, we solve the IR-cut SD equation and obtain the corresponding solution $M_{\rm IR}(p^2;\Lambda_{\rm IR})$. We show in fig. 6(a) the infrared quark mass $M_{\rm IR}(0;\Lambda_{\rm IR})$ plotted against the IR cutoff $\Lambda_{\rm IR}$. For $\Lambda_{\rm IR} < 0.35$ GeV, no significant effect is observed for DCSB, according to the infrared vanishing of the SD kernel. In contrast, a significant mass reduction appears for $\Lambda_{\rm IR} > 0.4\,{\rm GeV}$, and no DCSB is observed as $M_{\rm IR}(p^2;\Lambda_{\rm IR}) = 0$ for $\Lambda_{\rm IR} > \Lambda_{\rm IR}^{\rm crit} \simeq 0.53\,{\rm GeV}$. These results seem to indicate the relevant role of the infrared region as $0.4\,{\rm GeV} < p < 0.53\,{\rm GeV}$ for DCSB. Figure 6(b) shows the IR-cut SD kernel function for $\Lambda_{\rm IR}^{\rm crit}$, which is the critical value on DCSB.

Finally, we investigate the role of the IM enhancement of the SD kernel for DCSB. The SD kernel function $K(p^2)$ obtained from the lattice QCD data of the quark propagator indicates the IM enhancement, and takes a maximal value $K_{\max} = 38.76$ at $p^2 \simeq 0.368\,\mathrm{GeV}^2 \simeq (0.607\,\mathrm{GeV})^2$ in the present analysis. (See fig. 4.) Here, we examine the IM-suppressed SD kernel function,

$$K_{\mathrm{IM}}(p^2; c) \equiv \mathrm{Min}(K(p^2), cK_{\max}), \tag{27}$$

with a real and positive constant c. For each c, we calculate the quark mass function $M_{\mathrm{IM}}(p^2; c)$ using the SD equation (14) with the modified kernel $K_{\mathrm{IM}}(p^2; c)$. We show in fig. 7(a) the infrared quark mass $M_{\mathrm{IM}}(0; c)$ plotted against c. Of course, for $c \geq 1$, one finds $K_{\mathrm{IM}}(p^2; c) = K(p^2)$ and $M_{\mathrm{IM}}(p^2; c) = M(p^2)$. As c decreases from 1, $M_{\mathrm{IM}}(p^2; c)$ rapidly decreases, and no DCSB is found as $M_{\mathrm{IM}}(p^2; c) = 0$ for $c < c_{\mathrm{crit}} \simeq 0.58$. Figure 7(b) shows the IM-suppressed SD kernel function for c_{crit}, which is the critical value on DCSB. This would indicate that the intermediate enhancement of the SD kernel in the region of $0.2\,\mathrm{GeV}^2 < p^2 < 0.8\,\mathrm{GeV}^2$, *i.e.*, $0.4\,\mathrm{GeV} < p < 0.9\,\mathrm{GeV}$, plays an important role for DCSB.

From the above three analyses, the relevant momentum region for DCSB is considered to be the IR and the IM regions as

$$0.4\,\mathrm{GeV} < p < 1.5\,\mathrm{GeV}. \tag{28}$$

6 Chiral symmetry at finite temperature

Finally, we demonstrate a simple application of the lattice-QCD–based SD equation to chiral symmetry restoration in finite-temperature QCD, using the Matsubara imaginary-time formalism.

In this formalism, the quark field $q(\mathbf{x}, \tau)$ and the gluon field $A_\mu(\mathbf{x}, \tau)$ at a finite temperature T obey the anti-periodic and periodic boundary condition in the imaginary-time direction, respectively, as

$$\begin{aligned} q(\mathbf{x}, \tau + 1/T) &= -q(\mathbf{x}, \tau), \\ A_\mu(\mathbf{x}, \tau + 1/T) &= A_\mu(\mathbf{x}, \tau). \end{aligned} \tag{29}$$

Accordingly, the temporal momentum variable p_0 is discretized to be the Matsubara frequency,

$$\begin{aligned} p_0 &\to (2n+1)\pi T \equiv \omega_n \quad \text{for quarks}, \\ p_0 &\to 2n\pi T \qquad\qquad\ \ \text{for gluons}, \end{aligned} \tag{30}$$

and the corresponding integration over p_0 becomes the summation over the Matsubara frequencies as

$$\int_{-\infty}^{\infty} \frac{\mathrm{d}p_0}{2\pi} \to T \sum_{n=-\infty}^{\infty} \tag{31}$$

in the SD equation.

As a result, the SD equation for the thermal quark mass function $M_T(\mathbf{p}^2, \omega_n^2)$ of the Matsubara frequency $\omega_n \equiv (2n+1)\pi T$ is given as

$$\begin{aligned} \frac{M_T(\mathbf{p}^2, \omega_n^2)}{Z(\omega_n^2 + \mathbf{p}^2)} &= 3C_F T \sum_{m=-\infty}^{\infty} \int \frac{\mathrm{d}^3 q}{(2\pi)^3} \\ &\times \frac{Z((\omega_n - \omega_m)^2 + (\mathbf{p}-\mathbf{q})^2) M_T(\mathbf{q}^2, \omega_m^2)}{\omega_m^2 + \mathbf{q}^2 + M_T(\mathbf{q}^2, \omega_m^2)} \\ &\times \frac{K((\omega_n - \omega_m)^2 + (\mathbf{p}-\mathbf{q})^2)}{(\omega_n - \omega_m)^2 + (\mathbf{p}-\mathbf{q})^2}. \end{aligned} \tag{32}$$

Here, $M_T(\mathbf{p}^2, \omega_n^2)$ depends only on $\mathbf{p}^2$ and ω_n^2, because of the three-dimensional rotational invariance and the imaginary-time reversal invariance of the system.

Using the kernel function $K(p^2)$ obtained in sect. 4, we solve the thermal SD equation (32) for $M_T(\mathbf{p}^2, \omega_n^2)$. We find that the quark wave function renormalization effect is rather small for the mass function $M_T(\mathbf{p}^2, \omega_n^2)$ and also the critical temperature T_c. Therefore, we set $Z(p^2) = 1$ in the following calculation for simplicity, considering inaccuracy of the present lattice data for the wave function renormalization $Z(p^2)$.

Figure 8 shows the numerical result for the thermal infrared quark mass $M_T(\mathbf{p}^2 = 0, \omega_0^2)$ plotted against the temperature T. Chiral symmetry restoration is found at a critical temperature $T_c \simeq 110\,\mathrm{MeV}$, which seems rather small in comparison with the critical temperature $T_c = 260$–$280\,\mathrm{MeV}$ of the quenched QCD phase transition [29].

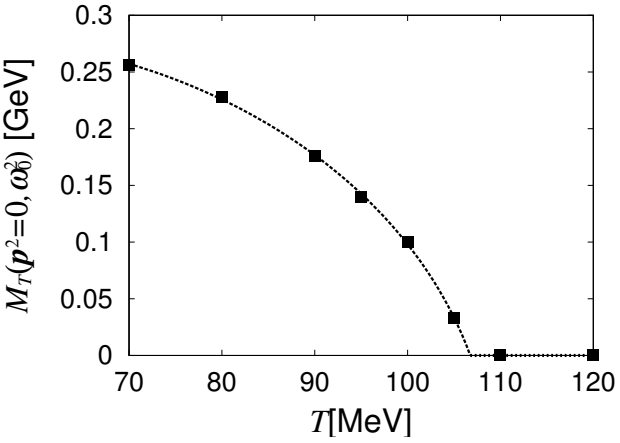

Fig. 8. (a) The thermal infrared quark mass $M_T(\mathbf{p}^2 = 0, \omega_0^2)$ plotted against the temperature T. Chiral symmetry restoration is found at a critical temperature $T_c \simeq 110\,\mathrm{MeV}$.

Figure 9 shows the thermal quark mass function $M_T(\mathbf{p}^2, \omega_n^2)$ at various Matsubara frequencies at a low temperature $T = 0.6T_c = 60\,\mathrm{MeV}$ and at a high temperature $T = 0.9T_c = 90\,\mathrm{MeV}$. One finds the following tendencies for the thermal quark mass $M_T(\mathbf{p}^2, \omega_n^2)$.

1. At fixed T, $M_T(\mathbf{p}^2, \omega_n^2)$ is a decreasing function of $\mathbf{p}^2$ for each Matsubara frequency n, and $M_T(\mathbf{p}^2, \omega_n^2)$ decreases with ω_n^2 for each value of $\mathbf{p}^2$.
2. For fixed n and $\mathbf{p}^2$, $M_T(\mathbf{p}^2, \omega_n^2)$ decreases with the temperature T.

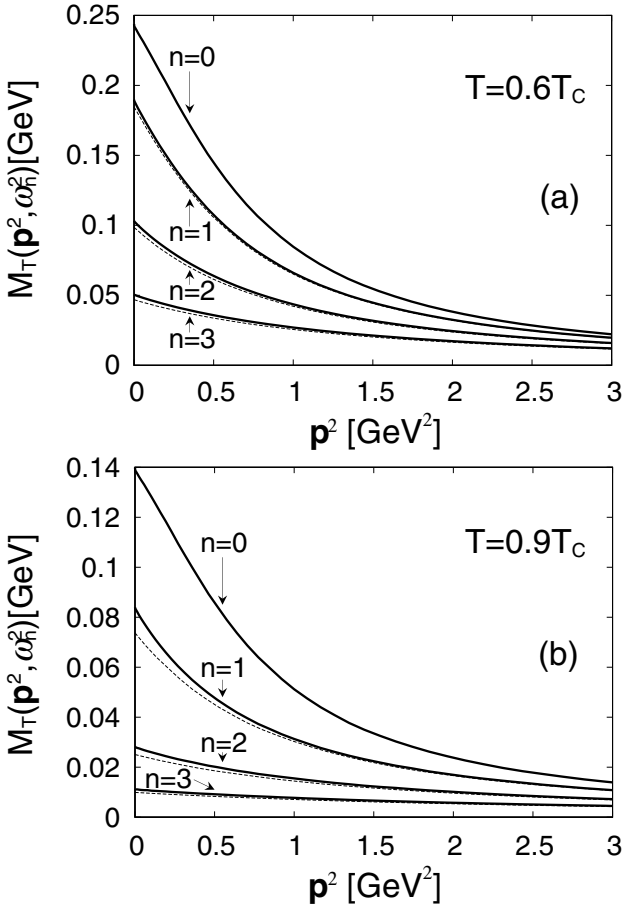

Fig. 9. The thermal quark mass function $M_T(\mathbf{p}^2, \omega_n^2)$ at various Matsubara frequencies $n = 0, 1, 2, 3$ obtained from the thermal SD equation for (a) a low-temperature case of $T = 0.6T_c \simeq 60\,\mathrm{MeV}$ and (b) a high-temperature case of $T = 0.9T_c \simeq 90\,\mathrm{MeV}$. For comparison, we add $M_T(\mathbf{p}^2+\omega_n^2-\omega_0^2, \omega_0^2)$ by the dashed curves.

As an interesting dependence of ω_n^2 and $\mathbf{p}^2$, we find at each T the "covariant-like relation" [30] for the thermal quark mass function as

$$M_T(\mathbf{p}^2, \omega_n^2) \simeq \tilde{M}_T(\mathbf{p}^2 + \omega_n^2) = \tilde{M}_T(\hat{p}^2). \qquad (33)$$

Here, $\hat{p}^2 \equiv \mathbf{p}^2 + \omega_n^2 = \mathbf{p}^2 + \{(2n+1)\pi T\}^2$ corresponds to the four-dimensional momentum squared, $p^2 = \mathbf{p}^2 + p_0^2$, and actually reduces into p^2 at $T = 0$. For the demonstration of the relation in eq. (33), we compare $M_T(\mathbf{p}^2, \omega_n^2)$ with $M_T(\mathbf{p}^2 + \omega_n^2 - \omega_0^2, \omega_0^2)$ in fig. 9, and find an approximate coincidence of $M_T(\mathbf{p}^2, \omega_n^2) \simeq M_T(\mathbf{p}^2 + \omega_n^2 - \omega_0^2, \omega_0^2)$ at each n even near the critical temperature T_c.

In this calculation, we have included only the (anti-) periodicity in the imaginary-time direction, and have ignored the nontrivial thermal effects on the quark and gluon propagators and vertex functions. Nevertheless, we observe chiral symmetry restoration at high temperature and obtain a rough estimate of the critical temperature. For more consistent calculation, it would be interesting to use the lattice QCD results on the quark and gluon propagators at finite temperature.

7 Summary and concluding remarks

We have investigated the Schwinger-Dyson (SD) formalism based on lattice QCD data, and have studied dynamical chiral-symmetry breaking (DCSB) in QCD. We have extracted the SD kernel function $K(p^2)$, which is the product of the quark-gluon vertex and the polarization factor in the gluon propagator, in an Ansatz-independent manner from the quenched lattice data for the quark propagator in the Landau gauge. We have found that the SD kernel $K(p^2)$ exhibits infrared vanishing and a large enhancement at the intermediate-energy region around $p \sim 0.6\,\mathrm{GeV}$.

We have investigated the relation between the quark mass function and the SD kernel, considering the important scale region for DCSB. Detailed examination has revealed that the infrared and the intermediate energy regions as $0.4\,\mathrm{GeV} < p < 1.5\,\mathrm{GeV}$ would be relevant for DCSB. The "intermediate kernel enhancement" is found to be also important for DCSB.

We have applied the lattice-QCD–based SD equation to thermal QCD, and have calculated the quark mass function at the finite temperature. We have found that spontaneously broken chiral symmetry is restored at the high temperature above 110 MeV.

In this paper, we have mainly investigated DCSB with the SD equation in the Landau gauge. It is however interesting to study the possible relation between DCSB and color confinement in the SD formalism. To this end, it is also meaningful to investigate the SD equation in other choices of the gauge such as the maximally Abelian (MA) gauge [31]. Actually, the dual Ginzburg-Landau theory, a model of QCD in the MA gauge [32], indicates that DCSB is caused by the strong enhancement of the Abelian gluon propagator due to monopole condensation [15], which leads to quark confinement. In a similar context, the authors in ref. [16] demonstrated with the $SU(2)$ lattice gauge theory that the intermediate enhancement of the gluon polarization factor in the Landau gauge is mainly due to center vortices, which would be responsible to color confinement. In any case, to investigate relations between DCSB and color confinement in our formalism is one of the interesting future subjects.

It is interesting to apply these formalisms to a finite-density system [27], since finite-density QCD is still rather difficult to be studied within the present lattice QCD ability.

In the near future, we expect that the combination of lattice QCD and the nonperturbative formalism such as the SD and the BS equations provides us a powerful tool to clarify nonperturbative aspects of hadron physics based on QCD [27,21]. In this framework, once accurate lattice QCD data are given, more reliable results can be obtained. Therefore, in order to establish this new framework, it is much desired to obtain more accurate data on the quark

and gluon propagators as well as quark-gluon vertex functions [22] in both quenched and full lattice QCD [18].

We would like to thank Profs. P. Tandy, C.D. Roberts and Y. Sumino, for their useful comments and discussions. This work was supported in part by Grant for Scientific Research ((B) No.15340072) from the Ministry of Education, Culture, Sports, Science and Technology, Japan. H.I. was supported by a 21st Century COE Program at Tokyo Institute of Technology "Nanometer-Scale Quantum Physics" by the Ministry of Education, Culture, Sports, Science and Technology.

Appendix A. Numerical extraction of the SD kernel

The problem to extract $K(p^2)$ from eq. (16) is categorized as the inverse problem, which is generally difficult in mathematics. Here, we show the detail on the numerical extraction of the SD kernel $K(p^2)$ from eq. (16).

First, we make the transformation of the variable from $(p^2, \tilde{q}^2)$ to (α, β), as $p^2 = \tan^\nu \alpha$ and $\tilde{q}^2 = \tan^\nu \beta$. One of the advantage of such a transformation is that we can map the infinite range of $p^2, \tilde{q}^2 \in [0, \infty]$ to the finite range of $\alpha, \beta \in [0, \pi/2]$. As another advantage, by changing the power ν in $p^2 = \tan^\nu \alpha$, we can adjust the "weight" on the representation points of the integral variable. In this case, we find that one of the most suitable solutions can be numerically obtained, when the power in $\tan^\nu \alpha$ is fourth, *i.e.*, $\nu = 4$. In fact, the SD equation (16) reads

$$\frac{M(\tan^4\alpha)}{Z(\tan^4\alpha)} = \int_0^{\pi/2} \mathrm{d}\beta \frac{4\tan^3\beta}{\cos^2\beta} \times \Theta(\tan^4\alpha, \tan^4\beta) K(\tan^4\beta). \quad \text{(A.1)}$$

Second we discretize the variables α, β. We must carefully choose the discretization number. If the discretization number is too small, the error due to the smallness of discretization number becomes large. On the other hand, if the discretization number is too large, the accuracy of the calculation in solving the simultaneous equation becomes worse. Therefore, we should seek for the appropriate discretization number N, and find that it is about 300 in this case. After making the discretization of α, β, we get the discretized SD equation,

$$\frac{M_n}{Z_n} = h \sum_{m=1}^{N} \frac{4\tan^3(mh)}{\cos^2(mh)} \Theta_{nm} K_m, \quad \text{(A.2)}$$

where $\alpha = nh$, $\beta = mh$, $h \equiv \frac{\pi/2}{N}$, $N \simeq 300$, $M_n \equiv M(\tan^4(nh))$, $Z_n \equiv Z(\tan^4(nh))$, $K_n \equiv K(\tan^4(nh))$ and $\Theta_{nm} \equiv \Theta(\tan^4(nh), \tan^4(mh))$. Then, we can solve the simultaneous equation (A.2) for K_n, and obtain the SD kernel $K(p^2)$.

It is worth mentioning that K_n takes a small value in the infrared region but seems rather noisy in the ultra-infrared region as $p^2 < 0.1\,\mathrm{GeV}^2$, since K_n in this region is not so important for the determination of the quark mass function. In such a case, we introduce an ultra-infrared cutoff for K_n.

After the numerical extraction of $K(p^2)$, we have confirmed that the obtained SD kernel $K(p^2)$ reproduces the lattice quark propagator by solving the SD equation. Therefore, this procedure certainly works well in this case.

References

1. Y. Nambu, G. Jona-Lasinio, Phys. Rev. **122**, 345 (1961).
2. K. Higashijima, Phys. Rev. D **29**, 1228 (1984); Prog. Theor. Phys. Suppl. **104**, 1 (1991).
3. V.A. Miransky, Sov. J . Nucl. Phys. **38**, 280 (1983); *Dynamical Symmetry Breaking in Quantum Field Theories*, (World Scientific, Singapore, 1993) p. 1.
4. Particle Data Group, Phys. Rev. D **66**, 010001 (2002).
5. J. Gasser, H. Leutwyler, Phys. Rep. **87**, 77 (1982).
6. T. Hatsuda, T. Kunihiro., Phys. Rep. **247**, 221 (1994) and references therein.
7. D. Diakonov, V. Petrov, Nucl. Phys. B **245**, 259 (1984).
8. For instance, H. Georgi, *Lie Algebras in Particle Physics* (Benjamin/Cummings, Menlo Park, 1982) p.1.
9. M. Bando, T. Kugo, K. Yamawaki, Phys. Rep. **164**, 217 (1988) and references therein.
10. M. Baker, K. Johnson, Phys. Rev. D **3**, 2516 (1971).
11. T. Maskawa, H. Nakajima, Prog. Theor. Phys. **52**, 1326 (1974); **54**, 860 (1975).
12. For a recent article, M. Hashimoto, M. Tanabashi, hep-ph/0210115 (2002) and references threin.
13. K.-I. Aoki, M. Bando, T. Kugo, M.G. Mitchard, H. Nakatani, Prog. Theor. Phys. **84**, 683 (1990); K.-I. Aoki, T. Kugo, M.G. Mitchard, Phys. Lett. B **266**, 467 (1991).
14. C.D. Roberts, A.G. Williams, Prog. Part. Nucl. Phys. **33**, 477 (1994); F.T. Hawes, C.D. Roberts, A.G. Williams, Phys. Rev. D **49**, 4683 (1994).
15. H. Suganuma, S. Sasaki, H. Toki, Nucl. Phys. B **435**, 207 (1995); S. Sasaki, H. Suganuma, H. Toki, Prog. Theor. Phys. **94**, 373 (1995); H. Suganuma, S. Sasaki, H. Toki, H. Ichie, Prog. Theor. Phys. Suppl. **120**, 57 (1995).
16. K. Langfeld, H. Reinhardt, J. Gattnar, Nucl. Phys. B **621**, 131 (2002); J. Gattnar, K. Langfeld, H. Reinhardt, Phys. Rev. Lett. **93**, 061601 (2004), hep-lat/0403011.
17. T. Doi, N. Ishii, M. Oka, H. Suganuma, Phys. Rev. D **67**, 054504 (2003); **70**, 034510 (2004).
18. P.O. Bowman, U.M. Heller, D.B. Leinweber, M.B. Parappilly, A.G. Williams, Phys. Rev. D **70**, 034509 (2004), hep-lat/0402032; F.D.R. Bonnet, P.O. Bowman, D.B. Leinweber, A.G. Williams, J.M. Zanotti, Phys. Rev. D **64**, 034501 (2001); F.D.R. Bonnet, P.O. Bowman, D.B. Leinweber, A.G. Williams, Phys. Rev. D **62**, 051501 (2000).
19. P.O. Bowman, U.M. Heller, A.G. Williams, Phys. Rev. D **66**, 014505 (2002); Nucl. Phys. B (Proc. Suppl.) **106**, 820 (2002); Nucl. Phys. A (Proc. Suppl.) **109**, 163 (2002).
20. F.D.R. Bonnet, P.O. Bowman, D.B. Leinweber, A.G. Williams, J.B. Zhang, Phys. Rev. D **65**, 114503 (2002).
21. M.S. Bhagwat, M.A. Pichowsky, C.D. Roberts, P.C. Tandy, Phys. Rev. C **68**, 015203 (2003).
22. J.-I. Skullerud, P.O. Bowman, A. kizilersu, D.B. Leinweber, A.G. Williams, JHEP **0304**, 047 (2003).

23. J.S. Ball, T.-W. Chiu, Phys. Rev. D **22**, 2542; 2550 (1980); **23**, 3085 (1981)(E).
24. D.C. Cartis, M.R. Pennington, Phys. Rev. D **42**, 4165 (1990).
25. C.S. Fisher, R. Alkofer, Phys. Rev. D **67**, 094020 (2003).
26. T. Kugo, M.G. Mitchard, Phys. Lett. B **282**, 162 (1992); **286**, 335 (1992).
27. H. Iida, M. Oka, H. Suganuma, Nucl. Phys. B (Proc. Suppl.) **129** & **130**, 602 (2004); *Proceedings of the International Workshop "QCD Down Under", Adelaide, March 2004*, to be published in Nucl. Phys. B (Proc. Suppl.) (2005).
28. P. Maris, P.C. Tandy, Phys. Rev. C **60**, 055214 (1999).
29. G. Boyd, J. Engels, F. Karsch, E. Laermann, C. Legeland, M. Lutgemeier, B. Petersson, Nucl. Phys. B **469**, 419 (1996); N. Ishii, H. Suganuma, H. Matsufuru, Phys. Rev. D **66**, 094506 (2002).
30. S. Sasaki, H. Suganuma, H. Toki, Phys. Lett. B **387**, 145 (1996).
31. K. Amemiya, H. Suganuma, Phys. Rev. D **60**, 114509 (1999).
32. H. Suganuma, K. Amemiya, H. Ichie, A. Tanaka, Nucl. Phys. A **670**, 40 (2000).